The Dissociation Kinetics of Energy-Selected $CpMn(CO)_3^+$ Ions Studied by Threshold Photoelectron−Photoion Coincidence Spectroscopy

Yue Li, Bálint Sztáray,† and Tomas Baer*

Contribution from the Department of Chemistry, University of North Carolina, Chapel Hill, North Carolina 27599-3290

Received November 20, 2000

Abstract: Threshold photoelectron−photoion coincidence spectroscopy has been used to investigate the dissociation kinetics of the cyclopentadienyl manganese tricarbonyl ion, $CpMn(CO)_3^+$. The ionization energy of $CpMn(CO)_3$ was measured from the threshold photoelectron spectrum to be 7.69 ± 0.02 eV. The dissociation of the $CpMn(CO)_3^+$ ion proceeds by the sequential loss of three CO molecules. The first and third CO loss reactions were observed to be slow (lifetimes in the microsecond range). By simulating the resulting asymmetric time-of-flight peak shapes and breakdown diagram, 0 K onsets for three product ions were determined to be 8.80 ± 0.04, 9.43 ± 0.04, and 10.51 ± 0.06 eV, respectively. Combined with the adiabatic ionization energy, the three successive Mn−CO bond energies in the $CpMn(CO)_3^+$ were found to be alternating with values of 1.11 ± 0.04, 0.63 ± 0.04, and 1.08 ± 0.06 eV, respectively. Using a scaled theoretical $Cp-Mn^+$ bond energy of 3.10 ± 0.10 eV and the combined results from theory and experiment, the 298 K gas-phase heat of formation of $CpMn(CO)_3$ is suggested to be −419 ± 15 kJ/mol. Based on this value, the 298 K heats of formation of $CpMn(CO)_3^+$, $CpMn(CO)_2^+$, $CpMnCO^+$, and $CpMn^+$ are 325 ± 15, 546 ± 15, 719 ± 15, and 938 ± 15 kJ/mol, respectively. By scaling theoretical calculated neutral bond energies with the experimental information derived in this study, the successive Mn−CO bond energies were estimated to be 1.88, 1.10, and 1.03 eV, respectively, while the Cp−Mn bond energy was found to be 2.16 eV. Comparison between the quantum chemical calculations and experimental values shows that the loss of CO groups follows the lowest energy adiabatic path, in which electronic spin on the metal center is not conserved.

Introduction

The thermochemistry of organometallic compounds is an intriguing subject because the low-lying metal d electrons participate in bonding schemes that have no counterparts in ordinary organic compounds.[1] A knowledge of metal−carbon and metal−hydrogen bond enthalpies is essential for the understanding of catalytic reaction mechanisms, which often involve the formation or the cleavage of those bonds.[2]

Tricarbonyl cyclopentadienyl manganese [$C_5H_5Mn(CO)_3$ or $CpMn(CO)_3$] is an archetypal η^5-bonded compound that has been used in catalytic reactions[3] as well as in chemical vapor deposition reactions.[4] This molecule is a thermally stable, relatively volatile, and low-melting-point solid. The physical and chemical properties of these π-bonded compounds have been extensively investigated[5] with major emphasis on the bonding and reactions of the cyclopentadienyl ring system.[6] $CpMn(CO)_3$ has been fully characterized by numerous physical techniques including vibrational (IR and Raman) spectroscopy,[7] microwave spectroscopy,[8] X-ray diffraction,[9] vapor-phase far-infrared spectroscopy,[10] and photoelectron studies[11,12] as well as molecular orbital calculations.[13−15]

The microwave[8] and X-ray diffraction[9] studies of $CpMn(CO)_3$ have indicated that the C_5 and C_3 axes of the π-C_5H_5 and $Mn(CO)_3$ groups are coincident, and the C_5H_5 ring is nearly symmetrical and lies parallel to the plane formed by three oxygen atoms. Lichtenberger et al.[11,12] published the first gas-phase photoelectron spectrum of the compound. On the basis of electron ionization mass spectra of $CpMn(CO)_3$, several groups reported ionization energies and fragment ion appearance energies.[16−19] The results show that the simple bond rupture

† Present address: Department of General and Inorganic Chemistry, Eötvös Loránd University, Budapest, Hungary.

(1) Skinner, H. A. Historical perspective of organometallic thermochemistry. In *Energetics of organometallic species*; Martinho Simoes, J. A., Ed.; Kluwer: Dordrecht, 1991; pp 1−8.
(2) Martinho Simões, J. A.; Beauchamp, J. L. *Chem. Rev.* **1990**, *90*, 629−688.
(3) Liu, H. P.; George, G. A. *Polymer* **1996**, *37*, 3675−3682.
(4) Almond, M. J.; Redman, H.; Rice, D. A. *J. Mater. Chem.* **2000**, *10*, 2842−2846.
(5) Frigyes, D.; Szepes, L. *J. Organomet. Chem.* **1998**, *563*, 147−152.
(6) Wilkinson, G.; Stone, F. G. A.; Abel, E. W. *Comprehensive Organometallic Chemistry*; Pergamon Press: Oxford, 1982.
(7) Parker, D. J.; Stiddard, M. H. B. *J. Chem. Soc., A* **1970**, 480.
(8) Tyler, J. K.; Cos, A. P.; Sheridan, J. *Nature* **1959**, *183*, 1182.
(9) Berndt, A. F.; Marsh, R. E. *Acta Crystallogr.* **1963**, *16*, 118.
(10) Mahmood, Z.; Hussain, I.; Ellis, A. M.; Russell, D. K. *Spectrochim. Acta, Part A* **1997**, *53*, 995−1003.
(11) Calabro, D. C.; Hubbard, J. L.; Blevins, C. H. I.; Campbell, A. C.; Lichtenberger, D. L. *J. Am. Chem. Soc.* **1981**, *103*, 6839−6846.
(12) Lichtenberger, D. L.; Fenske, R. F. *J. Am. Chem. Soc.* **1976**, *98*, 50−63.
(13) Brown, D. A.; Fitzpatrick, N. J.; Mathews, N. J. *J. Organomet. Chem.* **1975**, *88*, C27−C29.
(14) Fitzpatrick, N. J.; Savariault, J. M.; Labarre, J. F. R. *J. Organomet. Chem.* **1977**, *127*, 325−335.
(15) Schilling, B. E. R.; Hoffmann, R.; Lichtenberger, D. L. *J. Am. Chem. Soc.* **1979**, *101*, 585−591.
(16) Winters, R. E.; Kiser, R. W. *J. Organomet. Chem.* **1965**, *4*, 190−197.
(17) Muller, J.; Herberhold, M. *J. Organomet. Chem.* **1968**, *13*, 399−410.
(18) Efraty, A.; Huang, M. H. A.; Weston, C. A. *Inorg. Chem.* **1975**, *14*, 2796−2799.
(19) Sizoi, V. F.; Nekrasov, Y. S. *Bull. Acad. Sci. USSR* **1982**, *31*, 260−266.

10.1021/ja004019d CCC: $20.00
Published on Web 08/31/2001

prevails in the cyclopentadienyl metal carbonyls, but that some fragmentation of the C_5H_5 group also occurs.

The electron ionization results do not lead to accurate ion energetics because the sample's thermal energy distribution was not taken into account, the energy resolution was insufficient, and the kinetic shift was neglected in the data analysis. In this study we report on the investigation of the gas-phase dissociation kinetics of $CpMn(CO)_3^+$ ions using threshold photoelectron−photoion coincidence (TPEPICO) spectroscopy, a technique for energy-selecting ions and determining the dissociation rate constants. These results, analyzed with the statistical theory of unimolecular reactions, provide an avenue for the extraction of accurate dissociation limits and thus bond energies, as well as heats of formation of neutral precursors and fragments.

Experimental Approach

The threshold photoelectron−photoion coincidence (TPEPICO) apparatus has been described in detail previously.[20] Briefly, room-temperature sample vapor was leaked into the experimental chamber through a 1.5 mm diameter inlet and then was ionized with vacuum ultraviolet (VUV) light from an H_2 discharge lamp dispersed by a 1 m normal incidence monochromator. The VUV wavelengths were calibrated using the hydrogen Lyman-α line. The ions and the electrons were extracted in opposite directions with an electric field of 20 V/cm. Threshold photoelectrons were selected by a steradiancy analyzer that consists of a flight tube with small apertures that stop energetic electrons with perpendicular velocity components. Further discrimination against the energetic electrons was provided by a hemispherical electrostatic sector analyzer, resulting in a ∼35 meV combined photon and electron energy resolution. The ions were accelerated to 100 eV in the first 5 cm long acceleration region, while a short second region accelerated the ions to 220 eV. The ions were detected after drifting through a 30 cm field-free drift region. The electrons and ions were detected with a channeltron electron multiplier and a multichannel plate detector, respectively. The electron and ion signals served as start and stop pulses for measuring the ion time-of-flight (TOF), and the TOF for each coincidence event was stored in a multichannel pulse height analyzer. TOF distributions were obtained in 1−48 h, depending on the photon intensity and the desired spectrum quality.

The PEPICO spectra were used for two purposes. First, the fractional abundances of the precursor and the product ions were measured as a function of the photon energy (breakdown diagram). Second, the product ion TOF distributions were measured at energies close to the dissociation limit. Slowly dissociating (metastable) ions decay in the first acceleration region. The resulting product ion TOF distribution is asymmetrically broadened toward long TOF. The asymmetric peak shapes can be analyzed to extract the ion decay rates as a function of ion internal energy. These two types of information were used together in the data analysis.

Cyclopentadienyl manganese tricarbonyl ($CpMn(CO)_3$, 98%, Strem Chemicals) was used without further purification.

Quantum Chemical Calculations

In the simulations for the experimental data, vibrational frequencies and rotational constants of the equilibrium structures and transition states for relevant neutral and ionic species are required. Thus, quantum chemical calculations were performed using the Gaussian 98 package.[21] The neutral or ionic $CpMn(CO)_3$, $CpMn(CO)_3^+$, $CpMn(CO)_2^+$, $CpMnCO^+$, and $CpMn^+$ structures were fully optimized at the Hartree−Fock (HF) and DFT (B3LYP) levels of theory with the LANL2DZ[22,23] and DZVP[24] basis sets. Stationary points were confirmed through the calculations of harmonic vibrational frequencies, which were also used to calculate the zero-point vibrational energies (ZPE). The structures and main parameters obtained at the B3LYP/LANL2DZ level are shown in Figure 1. These calculations were performed for several spin states of the molecules or ions. Although the vibrational frequencies and the geometries did not change much with the electron spin, the energies changed considerably. This issue is discussed in a later section on the dissociation energies.

Figure 1 shows that the $Mn(CO)_3$ group in neutral $CpMn(CO)_3$ has nearly C_{3v} symmetry, and its C_3 axis is almost coincident with the symmetrical axis of the C_5H_5 ring. This is in agreement with the microwave[8] and X-ray diffraction[9] experimental results. The major change in the geometry upon ionization of $CpMn(CO)_3$ is the lengthening of the Mn−CO bonds, which extend by an average of nearly 0.09 Å. By contrast, the Cp carbon atom bonds to the central Mn atom hardly vary, with perhaps a slight tendency to shorten. The $Mn(CO)_3$ group in the $CpMn(CO)_3^+$ ion has a somewhat distorted C_{3v} symmetry, in which the $C_{12}-Mn_{11}$ bond length is a little shorter than the other two C−Mn bond lengths. When a CO group is lost from the ion, the remaining two Mn^+−CO bonds lengthen a bit more (ca. 0.08 Å), while the Mn^+−C bonds to the Cp group lengthen by an average of 0.06 Å. The loss of the second CO group results in a longer Mn^+−CO bond length. The $Mn(CO)_2$ group of $CpMn(CO)_2^+$ has an approximate symmetry of the C_{2v} point group, while the MnCO group of $CpMnCO^+$ is almost linear. Here we assumed that the $Mn(CO)_n$ symmetries of the $CpMn(CO)_n^+$ ions ($n = 3 \rightarrow 1$) are C_{3v}, C_{2v}, and $C_{\infty v}$, respectively. These symmetries are required in the later RRKM calculations. Similar with the neutral, the symmetrical axes of the three ions are nearly coincident with that of C_5H_5.

Initial estimates of the transition-state structures and vibrational frequencies for the CO loss reactions were obtained by calculating the structures with one extended $Mn^+\cdots CO$ bond. This resulted in real frequencies, except for one imaginary frequency that corresponds to the manganese−carbonyl stretch vibration. Sums of states were calculated at several photon energies using the corresponding sets of vibrational frequencies in order to locate the variational transition state.[25−27] For reasons that are not clear, this calculation would not converge for TS_1, which corresponds to the first CO loss reaction. Thus, we used the $CpMn(CO)_3^+$ frequencies as starting points for obtaining the TS_1 frequencies. To use the same type of calculation for the molecular ion and the transition state, we used DFT for the molecular ion and its TS in the first CO loss, and HF frequencies for the product ions and TS for the subsequent CO loss steps. In all three cases, the calculated or assumed TS frequencies were only the starting points for the final frequencies, which were adjusted to fit the data. All the frequencies used in the energy distribution and RRKM calculations are shown in Table 1.

Results and Discussion

1. TOF Distributions and Breakdown Diagram. TOF mass spectra of $CpMn(CO)_3$ were collected in the photon energy range of 8.3 → 12.5 eV. Typical time-of-flight distributions are shown

(20) Baer, T.; Booze, J. A.; Weitzel, K. M. Photoelectron photoion coincidence studies of ion dissociation dynamics. In *Vacuum ultraviolet photoionization and photodissociation of molecules and clusters*; Ng, C. Y., Ed.; World Scientific: Singapore, 1991; pp 259−298.

(21) Frisch, M. J.; Trucks, G. W.; Schlegel, H. B.; Scuseria, G. E.; Robb, M. A.; Cheeseman, J. R.; Zakrzewski, V. G.; Montgomery, J. A.; Stratmann, R. E.; Burant, J. C.; Dapprich, S.; Millam, J. M.; Daniels, A. D.; Kudin, K. N.; Strain, M. C.; Farkas, Ö.; Tomasi, J.; Barone, V.; Cossi, M.; Cammi, R.; Mennucci, B.; Pomelli, C.; Adamo, C.; Clifford, S.; Ochterski, J.; Petersson, G. A.; Ayala, P. Y.; Cui, Q.; Morokuma, K.; Malick, D. K.; Rabuck, A. D.; Raghavachari, K.; Foresman, J. B.; Cioslowski, J.; Ortiz, J. V.; Baboul, A. G.; Stefanov, B. B.; Liu, G.; Liashenko, A.; Piskorz, P.; Komáromi, I.; Gomperts, R.,; Martin, R. L.; Fox, D. J.; Keith, T.; Al-Laham, M. A.; Peng, C. Y.; Nanayakkara, A.; Gonzalez, C.; Challacombe, M.; Gill, P. M. W.; Johnson, B. G.; Chen, W.; Wong, M. W.; Andres, J. L.; Head-Gordon, M.; Replogle, E. S.; Pople, J. A. *Gaussian 98*, Revision A.7; Gaussian, Inc.: Pittsburgh, PA, 1998.

(22) Wadt, W. R.; Hay, P. J. *J. Chem. Phys.* **1985**, *82*, 284.

(23) Dunning, T. H., Jr.; Hay, P. J. In *Modern Theoretical Chemistry*; Schaefer, H. F. I., Ed.; Plenum: New York, 1976; pp 1−28.

(24) Godbout, N.; Salahub, D. R.; Andzelm, J.; Wimmer, E. *Can. J. Chem.* **1992**, *70*, 560.

(25) Baer, T.; Hase, W. L. *Unimolecular Reaction Dynamics: Theory and Experiments*; Oxford University Press: New York, 1996.

(26) Wardlaw, D. M.; Marcus, R. A. *Adv. Chem. Phys.* **1988**, *70*, 231−263.

(27) Hase, W. L. *Chem. Phys. Lett.* **1987**, *139*, 389−394.

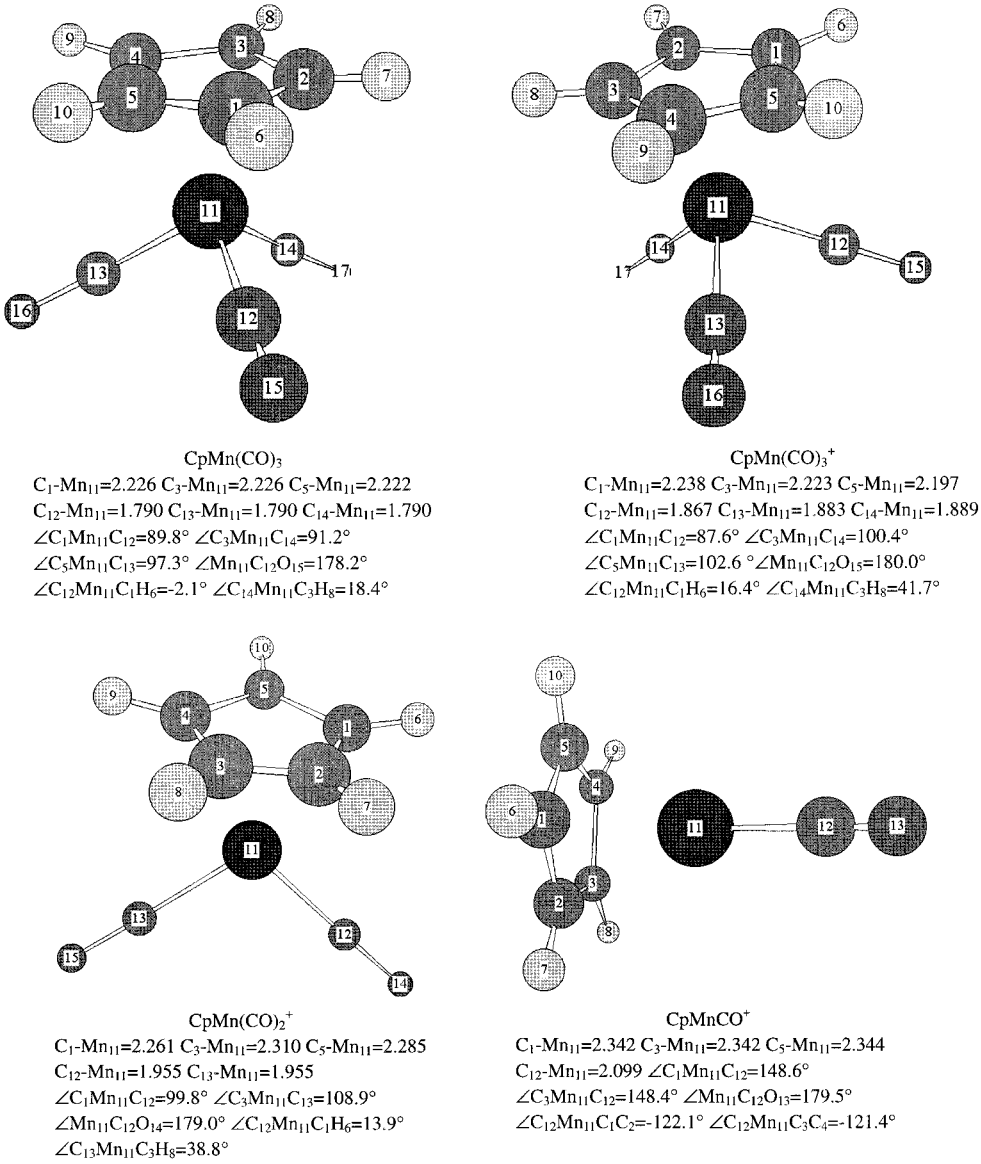

Figure 1. Lowest energy equilibrium structures of $CpMn(CO)_3$, $CpMn(CO)_3^+$, $CpMn(CO)_2^+$, and $CpMnCO^+$ (determined by density functional calculations at the B3LYP/LANL2DZ level). The spin multiplicity is 1 for $CpMn(CO)_3$, and 2, 4, and 6 for $CpMn(CO)_n^+$ ($n = 3 \rightarrow 1$), respectively.

Table 1. Frequencies Used in the Energy Distribution and RRKM Calculations

$CpMn(CO)_3$[a]	19, 83, 84, 97, 118, 123, 315, 317, 349, 380, 456, 456, 462, 507, 515, 575, 576, 606, 611, 638, 791, 800, 807, 810, 810, 877, 884, 969, 979, 1021, 1022, 1083, 1217, 1336, 1337, 1388, 1395, 1918, 1918, 1981, 3087, 3087, 3099, 3103, 3111
$CpMn(CO)_3^+$[a]	22, 70, 81, 93, 105, 117, 295, 305, 312, 335, 356, 375, 410, 425, 453, 455, 516, 542, 557, 564, 801, 804, 832, 852, 862, 916, 925, 976, 982, 1024, 1029, 1085, 1222, 1332, 1340, 1390, 1397, 2039, 2044, 2083, 3088, 3091, 3100, 3102, 3111
TS_1[b]	5, 41, 46, 54, 89, 117, 295, 305, 312, 335, 375, 410, 425, 453, 455, 516, 542, 557, 564, 801, 804, 832, 852, 862, 916, 925, 976, 982, 1024, 1029, 1085, 1222, 1332, 1340, 1390, 1397, 2039, 2044, 2083, 3088, 3091, 3100, 3102, 3111
$CpMn(CO)_2^+$[c]	27, 58, 72, 76, 191, 208, 245, 270, 280, 299, 310, 329, 349, 576, 584, 816, 822, 824, 832, 835, 895, 911, 972, 994, 1026, 1029, 1082, 1246, 1335, 1344, 1414, 1430, 2278, 2282, 3037, 3038, 3051, 3053, 3062
TS_2[d]	−17,[e] 9, 43(20), 55(26), 100(70), 101(71), 72, 208, 245, 268, 286, 326, 349, 568, 578, 814, 822, 823, 830, 832, 897, 898, 972, 988, 1025, 1027, 1077, 1245, 1336, 1338, 1410, 1422, 2202, 2290, 3038, 3039, 3051, 3053, 3062
$CpMnCO^+$[c]	13, 57, 200, 242, 266, 334, 338, 360, 590, 592, 827, 829, 830, 832, 835, 923, 928, 986, 987, 1032, 1034, 1084, 1245, 1361, 1362, 1420, 1422, 2292, 3042, 3042, 3054, 3055, 3064
TS_3[d]	−25,[e] 6, 6(11), 39(69), 39(69), 85(148), 292, 347, 507, 571, 778, 817, 823, 827, 832, 882, 895, 969, 985, 1024, 1025, 1074, 1245, 1332, 1336, 1405, 1418, 2200, 3039, 3040, 3051, 3053, 3062

[a] Calculated at the B3LYP/DZVP level. They were scaled by the factor 0.95.[28] [b] Assumed to be the same as $CpMn(CO)_3^+$ frequencies. The lowest frequency was treated as the internal rotation of Cp, and the next lowest four frequencies were adjusted to fit the TOF data. [c] Calculated at the HF/DZVP level. They were scaled by the factor 0.893.[29] [d] Calculated at the HF/DZVP level with the Mn−CO bond extended. They were scaled by the factor 0.893.[29] The lowest frequency was treated as the internal rotation of Cp, and the next lowest four non-negative frequencies were adjusted to fit the data. In the parentheses are the values before adjustment. [e] Reaction coordinate.

in Figure 2. In the figures, the ion peak at 33 μs is the precursor ion, $CpMn(CO)_3^+$ (*m*/*z* 204), whereas the product ions, $CpMn(CO)_2^+$ (*m*/*z* 176), $CpMnCO^+$ (*m*/*z* 148), and $CpMn^+$ (*m*/*z* 120), have TOF peaks at 30.7, 28.1, and 25.4 μs, respectively. The points correspond to experimental data, while the solid line corresponds to the fitted TOF distributions as discussed in the following section. It can be seen in Figure 2 that the precursor ion peak consists of two parts, a central peak on top of a broader

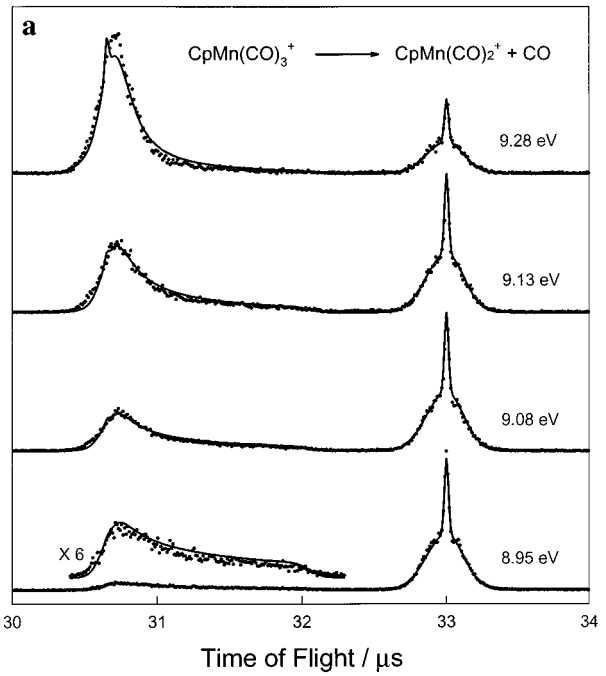

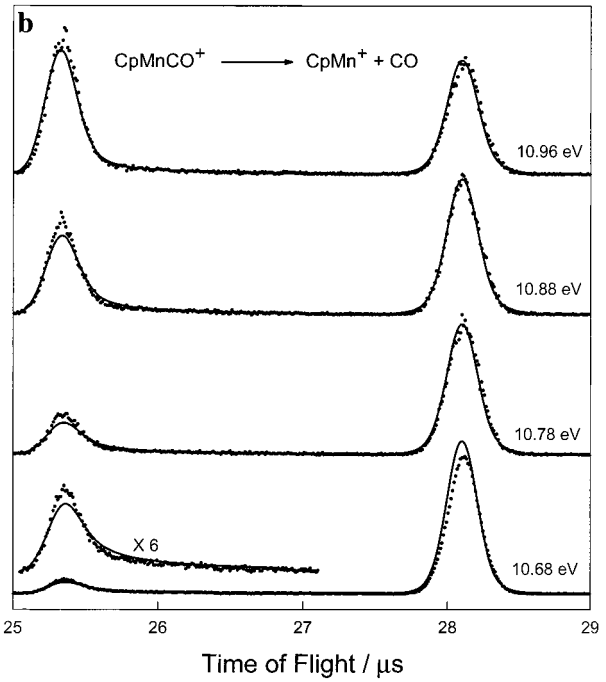

Figure 2. (a) Ion TOF distributions at selected photon energies for the first CO loss reaction. The points are the experimental data, and the solid lines are the simulation results. The asymmetric $CpMn(CO)_2^+$ peak at 30.7 μs is due to the slow CO loss reaction. (b) Ion TOF distributions at selected photon energies for the third CO loss reaction. The points are the experimental data, and the solid lines are the simulation results. The asymmetric $CpMn^+$ peak at 25.4 μs is due to the slow CO loss reaction.

one. The sharp part results from the effusive jet produced by the sample inlet, while the broad peak results from the $CpMn(CO)_3$ vapor in the background. The simulation takes this into account, and a vestige remains in the CO loss peak at 9.28 eV. But kinetic energy release broadens out this sharp peak. The results, which agree with earlier electron ionization studies,[16−19] show that the primary fragmentation of $CpMn(CO)_3^+$ corresponds to stepwise loss of three mass number 28 ligands, i.e., CO. Below a photon energy of 9.0 eV the two peaks correspond

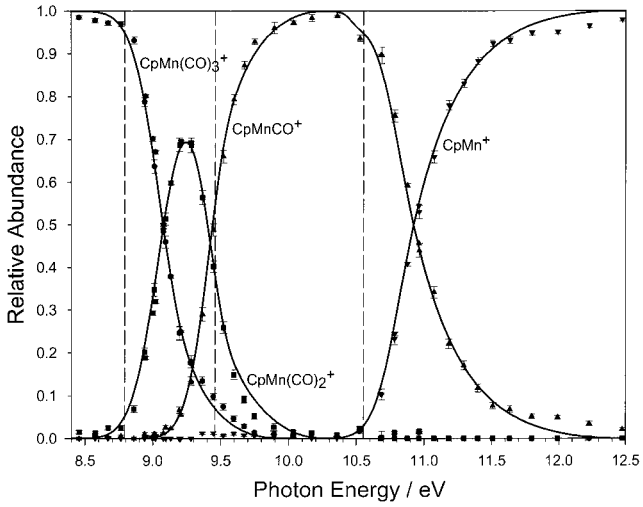

Figure 3. Breakdown diagram of $CpMn(CO)_3^+$. The points are the experimental data with error estimates, and the solid line is the simulation result by taking into account the internal energy distribution of the sample at 300 K, the Mn−CO bond energies, and the dissociation rate function $k(E)$. Vertical dashed lines indicate the derived 0 K dissociation onsets of the three consecutive CO loss reactions.

to the molecular ion, $CpMn(CO)_3^+$, and its first product ion, $CpMn(CO)_2^+$, respectively. At photon energies between 9.0 and 10.0 eV, $CpMnCO^+$, the product of two CO loss, can be seen as well. At photon energies in excess of 10.6 eV, the only two peaks correspond to the $CpMnCO^+$ and $CpMn^+$ ions.

Figure 3 shows the breakdown diagram of the $CpMn(CO)_3^+$ ion in which the ion fractional abundance is plotted as a function of the photon energy. The points are the experimental ratios with error estimates, while the solid lines show the simulation results and the vertical dashed lines indicate the location of the three 0 K dissociation onsets. The crossover energies, in which the abundances of precursor ion and product ion are equal to 50%, are 9.08, 9.44, and 10.93 eV. No cyclopentadienyl loss is observable in this study. The electron ionization experiments show that the appearance energy of Mn^+ is about 14.4 eV,[16−18] which is higher than the maximum value of the H_2 lamp (∼14.0 eV) used in this study.

The dissociation reaction mechanism of the $CpMn(CO)_3^+$ ions can be described by eq 1.

$$CpMn(CO)_3 \xrightarrow{\text{Ionization}} CpMn(CO)_3^+ \xrightarrow{TS_1} CpMn(CO)_2^+ + CO \xrightarrow{TS_2} CpMnCO^+ + 2CO \xrightarrow{TS_3} CpMn^+ + 3CO \quad (1)$$

The electron ionization experiments[16−19] obtained similar results, but their results showed very weak $CpMn(CO)_2^+$ ion signals. From the breakdown diagram in Figure 3, it can be seen that the dissociation onsets of the first and the second CO losses are very close; that is, $CpMn(CO)_2^+$ is apparently easy to dissociate to $CpMnCO^+$ and CO. Because the $CpMn(CO)_2^+$ ion is stable over only a small energy interval, the poor electron energy resolution in the electron ionization experiment would result in a very weak $CpMn(CO)_2^+$ signal.

As shown in Figure 2, for the first and the third carbonyl loss reactions, the product ion TOF distributions are asymmetric at the energies close to the appearance energies of those fragments. This indicates that the ions dissociate throughout the whole first acceleration region of the ion analyzer. If the average lifetime of the ions is comparable to the time it takes to traverse the acceleration regions (∼10.0 μs), the time-of-flight of the fragment ions is between the precursor and product ion TOF,

and a quasi-exponential shape is observed in the product ion peak. The decay rates can be determined from the analysis of the peak shapes. Those ions that dissociate after exiting the first acceleration region are counted as precursor ions. In slow reactions this relatively short time scale of the PEPICO experiment leads to the so-called kinetic shift.[30−32] That is, the observed dissociation onset does not correspond to the true dissociation energy, but is shifted to an energy at which the dissociation rate is fast enough to permit ions to dissociate in the acceleration region.

2. Data Analysis. The extraction of thermochemical data and bond energies from the experimental data requires a careful analysis of rates in terms of the ion energy distribution. Although the TPEPICO resolution is about 35 meV, the average thermal energy of $CpMn(CO)_3$ is 0.278 eV, and the distribution extends beyond 0.7 eV at room temperature. To properly fit the three consecutive dissociation reactions in eq 1, it is necessary to interpret the measured rate constants in terms of a distribution of $k(E)$, in which the energy extends over this thermal energy distribution. The procedure, described in detail by Sztáray and Baer,[28] involves convolutions of the thermal energy distribution with the electron analyzer function and the rate constants, $k(E)$, for the three dissociation channels. The electron analyzer function was measured from a threshold photoelectron spectrum (TPES) of a rare gas, NO, or acetylene, which have widely spaced energy levels. However, this is not quite adequate for all energies because its use implies a flat photoelectron spectrum in which all ion energies are produced with equal probability. At some photon energies, the onsets are in Franck−Condon gap regions so that energetic electrons become more important than is assumed by the measured analyzer function. Thus, some adjustment of this function is necessary in those cases.

3. The Simulations of the Breakdown Diagram and TOF Distributions. The statistical RRKM theory was used to calculate rate constants of the unimolecular dissociation of the $CpMn(CO)_3^+$ ion. The RRKM calculations were performed using the well-known formula[25]

$$k(E) = \frac{\sigma N^{\ddagger}(E - E_0)}{h\rho(E)} \qquad (2)$$

in which E_0 is the activation energy, $N^{\ddagger}(E - E_0)$ is the sum of states of the transition state from 0 to $E - E_0$, and $\rho(E)$ is the density of states of the ion measured from the bottom of the ion ground-state potential well. The Cp twist (the lowest frequency) for the three product ions was treated as an internal rotation because for a similar molecule system, $CpCo(CO)_2$,[28] the experimentally determined barrier height for this rotation was found to be only 3.35 meV,[33] just twice the zero-point energy of this vibrational mode. The $Mn(CO)_n$ ($n = 3 \rightarrow 1$) groups in the respective precursor ions have nearly C_{3v}, C_{2v}, and $C_{\infty v}$ symmetries, while for those variational transition states which have one extended Mn^+-CO bond, the symmetries are C_1, C_1, and $C_{\infty v}$, respectively. Thus, the symmetry parameters, σ, used in the RRKM calculations for the three consecutive dissociation reactions are 3, 2, and 1, respectively.

The ion TOF distribution and the breakdown diagram can be calculated using the following fixed information: the thermal energy distribution, the acceleration electric fields, and the acceleration and drift field distances. The adiabatic ionization energy of the $CpMn(CO)_3$ from our TPES measurements was 7.69 ± 0.02 eV, which is 0.36 eV lower than the vertical IE of 8.05 eV reported by Calabro et al.[11] By adjusting the dissociation limits, the lowest four TS vibrational frequencies which determine the entropy of activation (not including the frequency associated with the Cp ring rotation, since it was treated as an internal rotation), and to a limited extent the threshold electron analyzer function, the breakdown diagram and the TOF distributions can be simultaneously fitted. The transition-state frequencies of the $CpMn(CO)_3^+$ ion dissociation reaction were guessed by deleting the 356 cm^{-1} frequency, which is assigned as the manganese−carbonyl stretch vibration, from the precursor ion frequencies and multiplying the lowest four frequencies by a factor less than 1.0. These four frequencies were optimized in the simulation calculations. The optimized four frequencies are ones that turn into product rotations after the dissociation, and thus are reduced to zero as the ion proceeds toward products. This calculation method, described previously by Keister et al.[34] and Sztáray and Baer,[28] was used to extract the dissociation limits.

To aid convergence of the optimization procedure, the simulation was carried out in a stepwise fashion. First, a modified breakdown diagram was considered in which all product ions were summed. By simulating this breakdown diagram and the TOF distributions for the $CpMn(CO)_2^+$ ion, the energy barrier height (E_1) and the transition-state frequencies for the first dissociation reaction, as well as the threshold electron analyzer function, can be determined. Similarly, for the second CO loss reaction, the breakdown diagram was modified by combining the $CpMnCO^+$ and $CpMn^+$ ions. In this fitting, E_1, the transition-state frequencies of the first CO loss reaction, and the threshold electron analyzer function, which are obtained in the first simulation, were fixed. Only the energy barrier height (E_2) and the transition-state frequencies were adjusted until the breakdown diagram and TOF distributions were simultaneously fitted for TS_2. Finally, the full data set with E_1, E_2, and TS_1 and TS_2 frequencies fixed was simulated to obtain E_3 and the TS_3 frequencies.

The best fit to both the TOF distributions and the breakdown diagram was obtained with the following parameters: $E_1 = 1.11 \pm 0.04$ eV, $E_2 = 0.63 \pm 0.04$ eV, and $E_3 = 1.08 \pm 0.06$ eV. The simulated breakdown diagram and TOF distributions are shown in Figures 2 and 3. The RRKM calculated rate constants are plotted in Figure 4.

The uncertainties for the above-derived parameters were also studied. Since the frequencies of the transition states are estimated using those of the molecular ion or the structures with an Mn^+-CO distance of 5 Å, any variation of the frequencies should change the derived barrier heights. We tested the sensitivity of the derived dissociation energies to the assumed vibrational frequencies. The frequencies obtained from the optimization were adjusted by multiplying these by a factor (40% → 160%). As a result of the frequency variance, the optimized barrier heights were shifted by about 0.02−0.06 eV. However, any shift of barrier heights beyond 0.03 eV makes the quality of the simulated TOF distributions become significantly worse. We also varied the assumed internal rotational barrier of C_5H_5 by multiplying it by a factor of 50% → 200%,

(28) Sztáray, B.; Baer, T. *J. Am. Chem. Soc.* **2000**, *122*, 9219−9226.
(29) Pople, J. A.; Scott, A. P.; Wong, M. W.; Radom, L. *Isr. J. Chem.* **1993**, *33*, 345−350.
(30) Huang, F. S.; Dunbar, R. C. *J. Am. Chem. Soc.* **1990**, *112*, 8167−8169.
(31) Lifshitz, C. *Mass Spectrom. Rev.* **1982**, *1*, 309−348.
(32) Chupka, W. A. *J. Chem. Phys.* **1959**, *30*, 191−211.
(33) Roehrig, M. A.; Chen, Q. Q.; Haubrich, S. T.; Kukolich, S. G. *Chem. Phys. Lett.* **1991**, *183*, 84−88.
(34) Keister, J. W.; Baer, T.; Thissen, R.; Alcaraz, C.; Dutuit, O.; Audier, H.; Troude, V. *J. Phys. Chem. A* **1998**, *102*, 1090−1097.

Table 2. Comparison of the Calculated and Experimental 0 K Ionization Energy and Dissociation Energy Results (in eV)

		calcd			
energies	reactions	spin-conserved surface	adiabatic surface	this study	other
IE	$Mn \rightarrow Mn^+$	11.14	7.51	–	7.44[a]
	$CpMn(CO)_3 \rightarrow CpMn(CO)_3^+$	7.62	7.62	7.69 ± 0.02	7.6,[b] 8.05[c]
	$CpMn(CO)_2 \rightarrow CpMn(CO)_2^+$	7.08	6.86	6.92[d]	
	$CpMnCO \rightarrow CpMnCO^+$	6.38	6.40	6.45[d]	
	$CpMn \rightarrow CpMn^+$	5.38	6.63	6.50[d]	
D_0	$CpMn(CO)_3^+ \rightarrow CpMn(CO)_2^+ + CO$	1.47	0.89	1.11 ± 0.04	0.31,[e] 0.65,[f] 0.75[g]
	$CpMn(CO)_2^+ \rightarrow CpMnCO^+ + CO$	1.39	0.51	0.63 ± 0.04	0.91,[e] 0.69,[f] 0.75[g]
	$CpMnCO^+ \rightarrow CpMn^+ + CO$	1.40	1.14	1.08 ± 0.06	2.39,[e] 1.54,[f] 2.2[h]
	$CpMn^+ \rightarrow Cp + Mn^+$	9.25/4.39[i]	2.79	3.10 ± 0.10	3.65,[e] 3.4,[f] 3.9[h]
	$CpMn(CO)_3 \rightarrow CpMn(CO)_2 + CO$	2.01	1.66	1.88[j]	1.47,[k] 2.38[l]
	$CpMn(CO)_2 \rightarrow CpMnCO + CO$	2.09	0.97	1.10[j]	
	$CpMnCO \rightarrow CpMn + CO$	2.40	0.91	1.03[j]	
	$CpMn \rightarrow Cp + Mn$	3.49	1.91	2.16[j]	2.20,[k] 2.56[m]

[a] NIST thermochemical tables.[35] [b] NIST webbook derivation of adiabatic IE from PES of Calabro et al.[11] [c] Vertical ionization energy, Calabro et al.[11] [d] The ionization energies are obtained by subtracting the ion and neutral energies. [e] Efraty et al.[18] [f] Müller and Herberhold.[17] [g] Winters and Kiser[16] (the average of the first and second Mn−CO bond energies). [h] Winters and Kiser.[16] [i] Results for forming singlet and triplet Mn^+, respectively. [j] The quantum chemical calculation results after adjustment. The estimated errors are 0.20 eV. [k] Chipperfield et al.[36] (the average of the three Mn−CO bond energies). [l] Klassen et al.[37] [m] Ryan et al.[38]

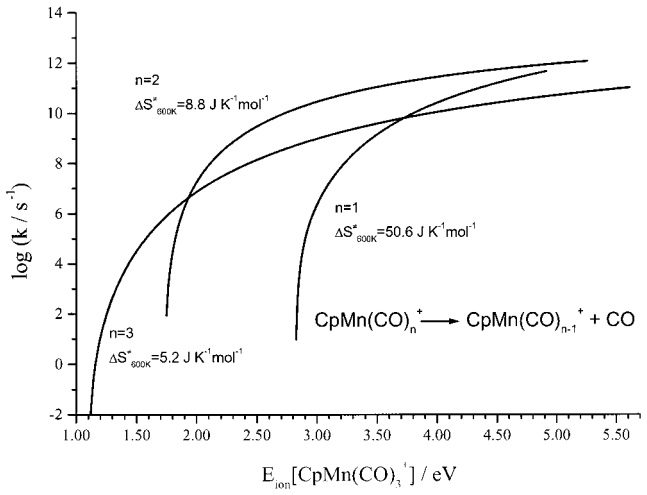

Figure 4. RRKM calculated dissociation rate curves of the three CO loss reactions.

and we found that all these tests resulted in barrier heights that agreed with the original one within 0.01 eV. The reason for this is undoubtedly a case of cancellation of errors because any variation in the "fixed" frequencies was compensated by a variation in the "adjustable" lowest four frequencies. This demonstrates that the rate constants depend mainly upon just two variables, the energy barrier height and the activation entropy. Taking into account the error limit of 0.02 eV associated with the ionization energy, we estimated the error limits to be 0.04, 0.04, and 0.06 eV for E_1, E_2, and E_3, respectively. The derived barriers correspond to dissociative photoionization limits of 8.80 ± 0.04, 9.43 ± 0.04, and 10.51 ± 0.06 eV for the loss of the first, second, and third CO ligand, respectively.

The comparison between these derived dissociation limits and the crossover energies in the breakdown diagram is interesting. The dissociation onsets for the first and third CO loss are 0.28 and 0.42 eV lower than the crossover energies, while the second dissociation onset is almost equal to its crossover energy. The ideal 0 K breakdown diagram exhibits sharp steps (down for the precursor ion and up for the fragment ion) at the dissociation onset. As discussed in detail by Sztáray and Baer,[28] the experimentally measured 298 K breakdown diagram shows the effects of the thermal energy distribution of the sample, the kinetic shift of slow dissociation reactions, and the imperfect instrumental resolution. The thermal energy shifts the crossover energy to a lower energy, while the kinetic shift moves the crossover energy to a higher energy. It is evident that the absence of a kinetic shift in the second CO loss reaction does not shift the observed onset to higher energy, so that its crossover energy is close to the 0 K onset.

The activation entropies of the three consecutive dissociation reactions of 5.2, 8.8, and 50.6 J·mol^{-1} K^{-1} at 600 K, respectively (as shown in Figure 4), are all positive, which indicates that these reactions proceed via loose transition states. This is characteristic of a simple bond-breaking reaction. The $k(E)$ curves in Figure 4 show that the rate constant for the loss of the first CO group increases more slowly than the rate constants for the other two reactions. This is a result of the lower entropy of activation. It is the low rate constant and its slow increase that result in a kinetic shift. The loss of the second CO group is associated with a much higher rate constant because the activation energy for this step is much smaller. In addition, the rate constant increases more rapidly because of the higher entropy of activation. As a result, the 0 K onset (dashed line in Figure 3) falls close to the crossover energy. The loss of the final CO group is also associated with a fast rate constant and a rapidly increasing one because of the large entropy of activation. However, the 0 K onset (dashed line in Figure 3) is again well below the crossover energy. This is because a significant amount of energy is lost as translational energy by the loss of the previous two CO groups. As a result, the crossover energy falls well above the 0 K onset. For the same reason, the slopes of the lines near the crossover energy (Figure 3) for the loss of the third CO group are considerably less than those of the two earlier CO losses.

4. Quantum Chemical Calculations of the Dissociation Energies. Table 2 lists the quantum chemical calculation results of the ionization energies and dissociation energies obtained at the B3LYP/6-311+G**//B3LYP/LANL2DZ level with zero-point energy corrections. The energy calculation of organometallic compounds is made difficult because of the large choice of electronic states associated with the metal center. In addition, there is very little spectroscopic information to serve as a guide. The only established fact is that the spin state of the Mn atom ($3d^54s^2$) in the ground state is $^6S_{5/2}$. However, what spin states should be chosen for species such as $CpMn(CO)_2^+$ or CpMn? According to the He(I) and He(II) PES studies,[38−40] there is

(35) Chase, M. W. *NIST−JANAF Thermochemical Tables*; American Institute of Physics: New York, 1998.
(36) Chipperfield, J. R.; Sneyd, J. C. R.; Webster, D. E. *J. Organomet. Chem.* **1979**, *178*, 177−189.

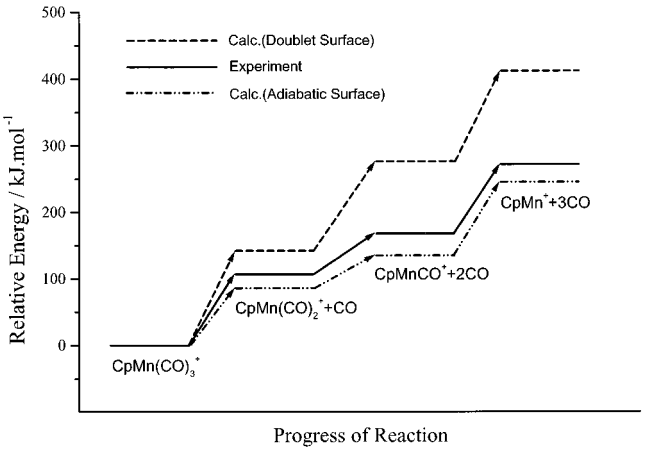

Figure 5. Comparison of experimental and calculated dissociation energies on the spin-conserved surface and the adiabatic surface.

evidence that manganocene, CpMnCp, is predominantly a high spin state (a sextet), unlike other metallocenes.

We have decided to consider two possible dissociation scenarios. One is the spin-conserved surface in which spin conservation is strictly followed. Because the spin quantum number of CO is zero, the loss of a CO group does not change the spin of the metal-containing species. Unlike CpMnCp, the HF and DFT calculations predict that the ground state of $CpMn(CO)_3$ is a singlet state, i.e., a low spin state. Thus, the sequential loss of CO from the neutral molecule, $CpMn(CO)_3$, results in only singlet states for the $CpMn(CO)_n$ fragments. Similarly, the loss of CO groups from the precursor ion results in only doublet states. The final loss of the Cp group (a doublet) from the neutral CpMn species will result in a doublet for the Mn atom. Similarly, for the ion, the final loss of the Cp group from a doublet $CpMn^+$ will result in either a singlet or a triplet Mn^+. The other surface is an adiabatic one in which the dissociation products follow the lowest energy path. Our calculations have determined the following most stable spin states. For neutral $CpMn(CO)_n$, the lowest energy spin states are 1, 3, 5, and 7 for $n = 3$, 2, 1, and 0, respectively. For the ionic species, $CpMn(CO)_n^+$, the lowest energy species have spin states 2, 4, 6, and 6, for $n = 3$, 2, 1, and 0, respectively. That is, high spin states are favored as ligands are lost.

The calculated energies for the spin-conserved and adiabatic dissociation channels are listed in Table 2. The experimentally derived bond energies for the ions as well as the experimentally determined ionization energy of the parent molecule are also listed in Table 2. By comparing the experimental and calculated bond energies for the ions, it is evident that the successive CO loss steps follow an adiabatic surface in which the spin states are not conserved. This is graphically illustrated in Figure 5. It can be seen that the adiabatic surface gives a better energy prediction than the spin-conserved surface. One of the remarkable results is the strongly alternating Mn^+-CO bond energies in the sequence $CpMn(CO)_n^+$ ($n = 3 \rightarrow 1$). The large drop from 1.11 to 0.63 eV is well predicted by the calculations on the adiabatic surface (Table 2), which show a decrease from 0.89 to 0.51 eV for $n = 3$ to 2, while on the spin-conserved surface, the second Mn^+-CO bond energy is almost equal to the third, and only a little lower than the first.

5. The $CpMn(CO)_3$ and $CpMn(CO)_3^+$ Thermochemistry. The experimental TPEPICO results provide information about differences between two ion states from which bond energies of $CpMn(CO)_3^+$ can be directly determined. However, to derive absolute heats of formation of the species involved, the heat of formation of at least one of the species must be known. In addition, to combine thermochemical values that are generally listed at 298 K with spectroscopic values as derived by the present TPEPICO experiment, we must convert the 298 K values to 0 K. The conversion from 298 to 0 K is done for the precursor molecule, $CpMn(CO)_3$, using the following equation:

$$\Delta_f H^\circ_{0K}[CpMn(CO)_3] = \Delta_f H^\circ_{298K}[CpMn(CO)_3] + [H^\circ_{298} - H^\circ_0](\text{elements}) - [H^\circ_{298} - H^\circ_0][CpMn(CO)_3] \quad (3)$$

in which "elements" refers to the sum of the elements in their standard states. In this case, it would be $8C(s) + {}^5/_2H_2 + {}^3/_2O_2 + Mn$, whose values are taken from Wagman et al.[41] The $[H^\circ_{298} - H^\circ_0][CpMn(CO)_3]$ value is obtained from ab initio MO or DFT calculated vibrational frequencies. If we take the experimental 298 K heat of formation of -481.9 ± 9 kJ/mol as listed in the NIST Webbook,[42] we obtain a 0 K value of -466 kJ/mol. A much better known energy is the heat of formation of the fully dissociated products, $Cp^\bullet + Mn^+ + 3CO$. By combining the measured ionization energy and the three Mn^+-CO bond energies with the heats of formation of the neutral precursor molecule and the fully dissociated products, we can derive the bond energy of the $Cp-Mn^+$ ion. This turns out to be 3.75 eV, a value that is clearly much larger than the calculated value of 2.79 eV. In addition, it is much larger than the average value of the $CpMnCp^+$ bond energies as reported by Ryan et al.,[38] who used the difference between the $CpMnCp^+$ heat of formation along with the heat of formation of the fully dissociated products, $2Cp^\bullet + Mn^+$ to derive an average bond energy of just 3.2 eV (310 ± 15 kJ/mol). In addition, there is evidence that the first loss of $Cp^\bullet$ from the ion is more endothermic than the loss of the second $Cp^\bullet$ ligand.[38]

It appears that the most uncertain value in the above calculation is the neutral heat of formation of $CpMn(CO)_3$. In fact, the NIST Webbook lists several values that differ by as much as 60 kJ/mol, and it is not clear that any one value is more reliable than another. So, let us assume that the heat of formation of $CpMn(CO)_3$ is essentially unknown and calculate a new value based on our results. We begin by assuming that the average error in the calculated bond energies of the ions is constant. The experimental energy for the loss of the three CO ligands from $CpMn(CO)_3^+$ is 2.82 eV, while the calculated value along the adiabatic surface is 2.54 eV, thereby yielding a scaling factor of 1.11. We now assume that the relative error in the calculated value is the same for the CO loss reactions as for the final loss of the $Cp^\bullet$ ligand. This scaled bond energy is then 3.10 eV. The error of this value is estimated to be 0.10 eV. This energy makes some sense in that it is slightly less than the average energy of 3.2 eV for the loss of both Cp units from $CpMnCp^+$ ion.[38] From this analysis we propose that the 298 K heat of formation of $CpMn(CO)_3$ should be raised by 0.65 eV or 63 kJ/mol to -419 kJ/mol. The related 0 K $\Delta_f H^\circ_{0K}$[CpMn-

(37) Klassen, J. K.; Selke, M.; Sorensen, A. A.; Yang, G. K. *J. Am. Chem. Soc.* **1990**, *112*, 1267−1268.
(38) Ryan, M. F.; Eyler, J. R.; Richardson, D. E. *J. Am. Chem. Soc.* **1992**, *114*, 8611−8619.
(39) Cauletti, C.; Green, J. C.; Kelly, M. R.; Powell, P.; Tilborg, J. V.; Robbins, J.; Smart, J. *J. Electron Spectrosc. Relat. Phenom.* **1980**, *19*, 327−353.
(40) Warren, K. D. *Struct. Bonding* **1976**, *27*, 45.
(41) Wagman, D. D.; Evans, W. H. E.; Parker, V. B.; Schum, R. H.; Halow, I.; Mailey, S. M.; Churney, K. L.; Nuttall, R. L. *The NBS Tables of Chemical Thermodynamic Properties*; J. Phys. Chem. Ref. Data Vol. 11, Suppl. 2; NSRDS, U.S. Government Printing Office: Washington, DC, 1982.
(42) http://webbook.nist.gov/chemistry/om/ (2000).

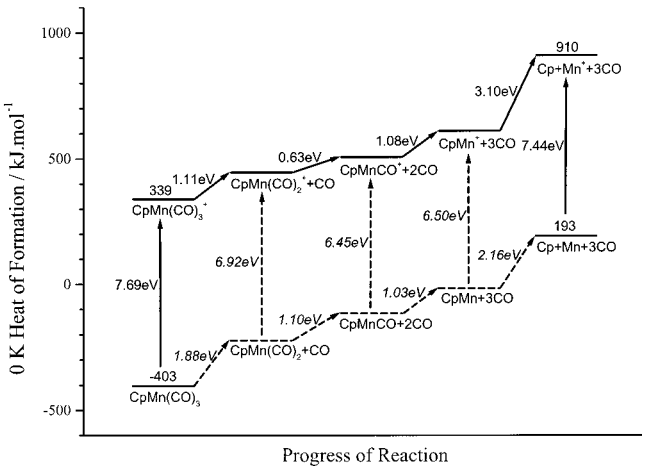

Figure 6. 0 K heat of formation diagram for the ionization and dissociation of the $CpMn(CO)_3$ system. The solid arrows show the experimentally determined energies, while the dashed arrows are energies in which the experimental values are used to scale the density functional calculations. The ionization energies of $CpMn(CO)_2$, CpMnCO, and CpMn are obtained by subtracting the ion and neutral energies. The spin multiplicities are assumed to be 1, 3, 5, and 7 for neutral $CpMn(CO)_n$ ($n = 3 \rightarrow 0$), and the spin multiplicity for Mn^+ is assumed to be 7.

Table 3. Experimental Thermochemical Values (in kJ/mol)[a]

species	$\Delta H_f^\circ{}_{(298K)}$	$\Delta H_f^\circ{}_{(0K)}$	$H^\circ_{298K} - H^\circ_{0K}$
$CpMn(CO)_3$	-419 ± 15[b]	-403 ± 15[c]	31.87[d]
$CpMn(CO)_3^+$	325 ± 15[b]	339 ± 15[c]	33.76[d]
$CpMn(CO)_2^+$	546 ± 15[b]	560 ± 15[c]	28.25[d]
$CpMnCO^+$	719 ± 15[b]	734 ± 15[c]	21.56[d]
$CpMn^+$	938 ± 15[b]	953 ± 15[c]	17.04[d]
Cp	241 ± 6[e]	252 ± 6[f]	15.25[d]
Mn	283.3 ± 4.2[g]	282.1 ± 4.2[g]	–
Mn^+	1006.986[g]	999.6 ± 0.5[g]	–
CO	-110.53[h]	-113.80[h]	8.665[h]

[a] In the $H^\circ_{298K} - H^\circ_{0K}$ calculations, the heat capacity of an electron was treated as 0.0 kJ/mol at all temperatures (the ion convention[43]). To convert to the electron convention, which treats the electron as a real particle, 6.197 kJ/mol should be added to the 298 K heat of formation each ion. [b] $\Delta H^\circ_{0K} \rightarrow \Delta H^\circ_{298K}$. [c] This study. [d] Determined in this study using DFT calculated vibrational frequencies. [e] Lias et al.[44] [f] $\Delta H^\circ_{298K} \rightarrow \Delta H^\circ_{0K}$. [g] NIST−JANAF thermochemical tables.[35] [h] Wagman et al.[41]

$(CO)_3$] is thus -403 kJ/mol. Although this seems like a drastic revision, it is in fact not unreasonable in light of the scatter in the reported values that range from -426 to -490 kJ/mol.[42] There is more support for this new value.

Figure 6 shows the 0 K heat of formation diagram for both the ionic and neutral dissociation reactions using this new $\Delta_f H^\circ_{0K}[CpMn(CO)_3]$. The energy associated with the complete dissociation to $Cp^\bullet + Mn + 3CO$ can be determined from the known heats of formation of the products listed in Table 3 and the assumed $\Delta_f H^\circ_{0K}[CpMn(CO)_3]$. This energy difference of 6.17 eV can be compared to the calculated value (adiabatic surface) of 5.45 eV (Table 2). The scaling factor in the neutral dissociation channels is $6.17/5.45 = 1.13$, which is very close to the scaling factor of 1.11 found in the ionic dissociation reactions. Finally, the scaled Cp−Mn bond energy is found to be 2.16 eV (209 kJ/mol). This can be compared to the suggested average value of 247 kJ/mol for the neutral Cp−Mn bond energy.[38] As with the ion, this value is based on the difference between the heats of formation of CpMnCp and the dissociation products, $2Cp^\bullet + Mn$.

The revised value for the heat of formation of $CpMn(CO)_3$ makes the calculations consistent with the experimental findings and makes the neutral and ion thermochemistry consistent with the reported heat of formation of CpMnCp.[44] We can also compare the resulting bond energies with those from other studies reported in the literature. The only experimental values for the ionic bond energies are ones determined by appearance energies in electron ionization studies.[16−18] As shown in Table 2, these values have quite an energy spread. The Mn^+−CO bond energy for the first CO loss is lower than that determined in our study. This is most likely due to the large thermal energy distribution that was not taken into account in their analysis of the appearance energy. Subsequent bond energies are higher than the ones determined in our study, especially for the case of the final Cp loss from $CpMn^+$. This discrepancy must be considered with some care because we did not measure this bond energy directly due to the inability of our light source to reach the Mn^+ ion appearance energy. In fact, it is precisely our raising of the $CpMn(CO)_3$ heat of formation that lowered our bond energy from 3.75 to 3.10 eV. The reason that we favor our lower bond energy is that the electron ionization measurements are expected to be too high for two reasons. First, it is apparent from the breakdown diagram in Figure 3 that the slope in the fragment ion signals for the first CO loss product is steeper than it is for subsequent CO loss steps, thereby making the determination of the onset more difficult and shifting it to higher energy. This is because of the energy partitioning in the dissociation reactions in which the neutral CO loss fragments carry away some of the ion internal energy. As a result, the subsequent ions are not nearly as energy selected as the initial $CpMn(CO)_3^+$ ion was. We take all of this into consideration in fitting our curves. The second reason the electron ionization onsets are expected to be too high is the kinetic shift. The loss of the Cp group has an activation energy of 3 eV, which means that the reaction at threshold will be immeasurably slow. The shift is expected to be on the order of 0.5 eV or even higher, depending on the vibrational frequencies of the transition state.

The literature contains very little information about the thermochemistry and ionization energy for neutral $CpMn(CO)_2$, CpMnCO, and CpMn. Static bomb calorimetry experiments on $CpMn(CO)_3$ by Chipperfield et al.[36] indicated that the average Mn−CO bond energy for the three Mn−CO bonds is 1.47 eV and the Cp−Mn bond energy is 2.20 eV. These results are remarkably close to ours (1.34 and 2.16 eV, respectively). The more recent solution-phase experiments of Klassen et al.[37] estimated the gas-phase value for the first Mn−CO bond energy to be 2.38 eV, a value that is 0.5 eV higher than ours (1.88 eV). Finally, there is the previously mentioned average Mn−Cp bond energy from CpMnCp of 2.56 eV.[38]

It can be seen in Figure 6 that the neutral species have higher Mn−CO bond energies than the ions except for CpMnCO. However, the bond energy of neutral CpMn is 0.94 eV lower than that of the $CpMn^+$ ion. The quantum chemical calculations in this study show that the highest occupied orbitals of CpMn are the d orbitals of Mn. The e_2'' orbitals of the Cp ring are of δ symmetry with respect to Mn[12] and will interact with these manganese d orbitals (d_{xy} and $d_{x^2-y^2}$) to form two antibonding orbitals. Therefore, the loss of the electron in these d orbitals will strengthen the Cp−Mn bond. However, $CpMn(CO)_n$ ($n = 3 \rightarrow 1$) compounds have different ionization mechanisms. When

(43) Rosenstock, H. M.; Draxl, K.; Steiner, B. W.; Herron, J. T. *Energetics of gaseous ions*; J. Phys. Chem. Ref. Data Vol. 6; American Chemical Society: Washington, DC, 1977.

(44) Lias, S. G.; Bartmess, J. E.; Liebman, J. F.; Holmes, J. L.; Levin, R. D.; Mallard, W. G. *Gas-Phase Ion and Neutral Thermochemistry*; J. Phys. Chem. Ref. Data Vol. 17, Suppl. 1; NSRDS, U.S. Government Printing Office: Washington, DC, 1988.

these neutral species are ionized, the electron in the bonding orbital (which is the e orbital[12] for $CpMn(CO)_3$) will be lost. Therefore, the ions will have fewer electrons for back-bonding, and thus the Mn−CO bond is weakened.

Conclusions

Threshold photoelectron−photoion coincidence (TPEPICO) spectroscopy has been used to investigate the dissociation kinetics of the cyclopentadienyl manganese tricarbonyl ion, $CpMn(CO)_3^+$. The ionization energy of $CpMn(CO)_3$ was measured from the threshold photoelectron spectrum to be 7.69 ± 0.02 eV. The dissociation of the $CpMn(CO)_3^+$ ion proceeds by the sequential loss of three CO molecules. By fitting the metastable ion time-of-flight distributions and the breakdown diagram with the statistical RRKM theory, accurate ion bond energies for all three Mn^+−CO bonds as well as the $Cp-Mn^+$ bond were obtained. A new value for the neutral heat of formation of $CpMn(CO)_3$ is derived by combining a calculated $Cp-Mn^+$ bond energy with the experimentally measured ionization energy and the three Mn^+−CO bond energies. This heat of formation, which is some 63 kJ/mol higher than the recommended value in the NIST Webbook, is now much more consistent with the CpMnCp heat of formation. The two heats of formation are linked because the two molecules form the same $CpMn^+$ product by dissociative ionization. Comparison between the quantum chemical calculations and experimental results shows that the loss of CO groups follows a lowest energy adiabatic path, in which electronic spin is not conserved. By combining the experimental results with density functional calculations of the corresponding neutral sequence of bond ruptures, it was possible to get reasonable neutral gas-phase $CpMn(CO)_3$ bond energies. The first Mn−CO bond energies in the ion and neutral species are 1.11 ± 0.04 and 1.88 ± 0.20 eV, respectively. An interesting drop in the second Mn−CO bond energy in the ion (0.63 ± 0.04 eV) is definitely not mirrored in its neutral counterpart (1.10 ± 0.20 eV). Although the Mn−CO bond energies are higher in the neutral molecule than they are in the ion, the Cp−Mn bond energy is much stronger in the ion (3.10 ± 0.10 eV) than in the neutral species (2.16 ± 0.20 eV).

Acknowledgment. We thank the North Carolina Supercomputer facility for a generous allotment of computer time. We acknowledge grants from the U.S. Department of Energy and from the National Science Foundation through its International Programs for Eastern Europe. B.S. acknowledges support of the Hungarian Secretary of Education (Grant Number FKFP 0162/1999).

JA004019D